Article

Field-Induced Ferrimagnetic State in a Molecule-Based Magnet Consisting of a Co Ion and a Chiral Triplet Bis(nitroxide) Radical

Youhei Numata, Katsuya Inoue, Nikolai Baranov, Mohamedally Kurmoo, and Koichi Kikuchi

J. Am. Chem. Soc., **2007**, 129 (32), 9902-9909• DOI: 10.1021/ja064828i • Publication Date (Web): 21 July 2007

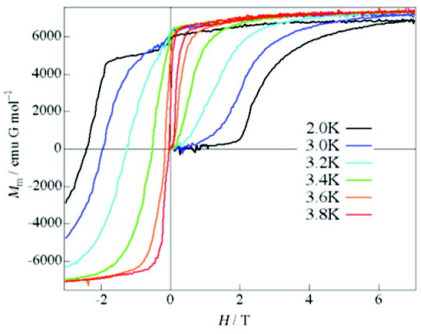

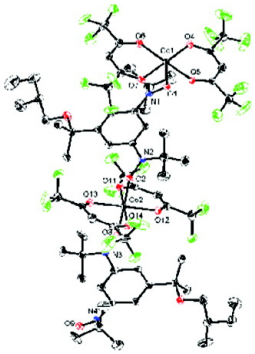

More About This Article

Additional resources and features associated with this article are available within the HTML version:

- Supporting Information
- Links to the 5 articles that cite this article, as of the time of this article download
- Access to high resolution figures
- Links to articles and content related to this article
- Copyright permission to reproduce figures and/or text from this article

View the Full Text HTML

J|A|C|S
ARTICLES
Published on Web 07/21/2007

Field-Induced Ferrimagnetic State in a Molecule-Based Magnet Consisting of a Co^{II} Ion and a Chiral Triplet Bis(nitroxide) Radical

Youhei Numata,[†,‡] Katsuya Inoue,*[,‡,§] Nikolai Baranov,[||] Mohamedally Kurmoo,[⊥] and Koichi Kikuchi[#]

Contribution from the Department of Structural Molecular Science, The Graduate University for Advanced Studies, Okazaki, 444-8585, Japan, Department of Chemistry, Faculty of Science, Hiroshima University, Kagamiyama, Higashi-Hiroshima 739-8526, Japan, Institute for Advanced Materials Research, Faculty of Science, Hiroshima University, Higashi-Hiroshima 739-8530, Japan, Institute of Metal Physics RAS and Ural State University, Ekaterinburg 620083, Russia, Laboratoire de Chimie de Coordination Organique, CNRS-UMR 7140, Université Louis Pasteur, 4 rue Blaise Pascal, 67000 Strasbourg Cedex, France, and Department of Chemistry, Tokyo Metropolitan University, Hachioji, Tokyo 192-0367, Japan

Received July 7, 2006; E-mail: kxi@hiroshima-u.ac.jp

Abstract: We present the synthesis, crystal structure, and temperature and field dependence of the magnetic properties of a new molecule-based magnet, $[Co(hfac)_2]$·BNO* (**1**), where hfac = 1,1,1,5,5,5-hexafluoroacetylacetonato and BNO* is the chiral triplet bis(nitroxide), 1,3-bis(*N*-*tert*-butyl-*N*-oxylamino)-5-{1′-methyl-1′-[2″-(*S*)-methylbutoxy]ethyl}benzene. The presence of enantiomer-pure BNO induces the formation of chiral one-dimensional chains that are packed parallel to each other in the noncentrosymmetric *P*1 space group. **1** exhibits four magnetic ground states: paramagnetic; antiferromagnetic; forced ferrimagnetic; field-induced metastable ferrimagnetic. In the paramagnetic state ($T > 20$ K), it presents short-range antiferromagnetic interaction between Co ion and nitroxide radical and has a minimum of $\chi_m T$ value at 220 K. The Weiss temperature estimated in the temperature range 220−300 K is found to be −89.9 K. At 20 K (T_N), an antiferromagnetic long-range ordering is established. In the temperature range 4 K $< T <$ 20 K, the isothermal magnetization curve show a spin-flip transition to the forced ferrimagnetic state at around 850 Oe. Below 4 K, this compound enters into a field-induced ferrimagnetic state, which is metastable and stabilized by the Ising character of the Co ion. In the low-temperature phase, the material becomes a very hard magnet with wide hysteresis loop whose coercive field reaches 25 kOe at 2 K. The magnetic phase diagram based on these magnetic data is presented.

Introduction

Molecule-based magnets have been investigated for several decades, not only for their molecular structures but also for the fact that their molecular arrangements and structural dimensionalities can be controlled. For example, pure organic radical magnets,[1] organic radical metal complexes,[2] and metal complexes bridged by nonmagnetic ligands such as oxalato,[3] azide,[4] polycarboxylic acids,[5] cyanide,[6] etc.,[7] are reported. They have various structures such as zero-dimensional clusters, one-dimensional chains, two-dimensional sheets, and three-dimensional networks. Among the large number of compounds,

[†] The Graduate University for Advanced Studies.
[‡] Faculty of Science, Hiroshima University.
[§] Institute for Advanced Materials Research, Hiroshima University.
[||] Institute of Metal Physics RAS and Ural State University.
[⊥] Université Louis Pasteur.
[#] Tokyo Metropolitan University.

(1) (a) *Molecular Magnetism, New Magnetic Materials*; Itoh, K., Kinoshita, M., Eds.; Kodansha: Tokyo, 2000. (b) *Magnetic Properties of Organic Materials*; Lahti, P. M., Ed.; Mercel Dekker Inc.: New York, 1995.
(2) (a) Miller, J. S.; Calabrese, J. C.; Rommelmann, H.; Chittipeddi, S. R.; Zhang, J. H.; Reiff, W. M.; Epstein, A. J. *J. Am. Chem. Soc.* **1987**, *109*, 769. (b) Benelli, C.; Caneschi, A.; Fabretti, A. C.; Gatteschi, D.; Pardi, L. *Inorg. Chem.* **1990**, *29*, 4153. (c) Iwamura H.; Inoue K. Magnetic Ordering in Metal Coordination Complexes with Aminoxyl Radicals. In *Magnetism: Molecules to Materials Vol. 2*; Miller, J. S., Drillon, M., Eds.; Wiley-VCH: Weinheim, Germany, 2001.
(3) (a) Girerd, J. J.; Kahn, O.; Verdaguer, M. *Inorg. Chem.* **1980**, *19*, 274. (b) Oshio, H.; Nagashima, U. *Inorg. Chem.* **1992**, *31*, 3295. (c) Decurtins, S.; Schmalle, H. W.; Oswald, H. R.; Linden, A.; Ensling, J.; Gütlich, P.; Hauser, A. *Inorg Chim. Acta* **1994**, *216*, 65. (d) Decurtins, S.; Schmalle, H. W.; Schneuwly, P.; Oswald, H. R. *Inorg. Chem.* **1993**, *32*, 1888.
(4) (a) Coryell, C. D.; Stitt, F. *J. Am. Chem. Soc.* **1940**, *62*, 2942. (b) Mallah, T.; Kahn, O.; Gouteron, J.; Jeannin, S.; Jeannin, Y.; O'Connor, C. J. *Inorg. Chem.* **1987**, *26*, 1375. (c) Escuer, A.; Cano, J.; Goher, M. A.; Journaux, Y.; Lloret, F.; Mautner, F. A.; Vicente, R. *Inorg. Chem.* **2000**, *39*, 4688. (d) Li, L.; Liao, D.; Jiang, Z.; Mouesca, J. M.; Rey, P. *Inorg. Chem.* **2006**, *45*, 7665.
(5) (a) Estes, E. D.; Estes, W. E.; Scaringe, R. P.; Hatfield, W. E.; Hodgson, D. J. *Inorg. Chem.* **1975**, *14*, 2564. (b) Ayyappan, P.; Evans, O. R.; Lin, W. *Inorg. Chem.* **2001**, *40*, 4627. (c) Zheng, Y.; Tong, M.; Zhang, W.; Chen, X. *Angew. Chem., Int. Ed.* **2006**, *45*, 6310.
(6) (a) Cushman, A. S. *Science* **1908**, *27*, 666. (b) Entley, W. R.; Girolami, G. S. *Science* **1995**, *268*, 397. (c) Verdaguer M.; Bleuzen A.; Marvaud V.; Vaissermann J.; Seuleiman M.; Desplanches C.; Scuiller A.; Train C.; Garde R.; Gelly G.; Lomenech C.; Rosenman I.; Veillet P.; Cartier C.; Villain F. *Coord. Chem. Rev.* **1999**, *190*−*192*, 1023. (d) Rogez, G.; Marvilliers, A.; Riviere, E.; Audiere, J.; Lloret, F.; Varret, F.; Goujon, A.; Mendenez, N.; Girerd, J.; Mallah, T. *Angew. Chem., Int. Ed.* **2000**, *39*, 2885. (e) Ohkoshi, S.; Arai, K.; Sato, Y.; Hashimoto, K. *Nat. Mater.* **2004**, *3*, 857. (f) Sieklucka, B.; Podgajny, R.; Przychodzen, P.; Korzeniak, T. *Coord. Chem. Rev.* **2005**, *249*, 2203.
(7) (a) Kahn, O. *Molecular Magnetism*; Wiley-VCH: New York, 1993.

 10.1021/ja064828i CCC: $37.00

discrete magnetic clusters and quasi one-dimensional magnetic chains are widely studied as candidates for single molecule magnets (SMMs)[8] and single chain magnets (SCMs),[9] respectively. These examples present very characteristic magnetic properties among the molecule-based magnets. They show unique magnetic hysteresis and relaxation properties on the basis of their molecular structures and magnetic anisotropy. One of their remarkable magnetic properties is magnetic quantum tunneling. This is the current focus of interest because these compounds are good examples where quantum phenomenon can be observed on a macroscale.

And as another remarkable feature of molecule-based compounds, the new materials, which have hybridized physical properties, can be constructed by the combination of two (or more) components which individually may have different properties. For example, some compounds designed from such ideas of combining magnetism and conductivity[10] or superconductivity[11] and magnetism and photoreactivity[12] and optical properties[13] are reported. In this respect, we have been interested in designing chiral molecule-based magnets with unique and novel magnetic properties. Here, we report the preparation, crystal structure, dc and ac magnetic properties, and the magnetic phase diagram of one of our designed chiral structured molecule-based magnets, $[Co(hfac)_2]$·BNO*, where the chirality is incorporated by the use of a chiral organic biradical. This approach has facilitated the production of several chiral structured magnets.[13] It is a novel antiferromagnetic compound $[Co(hfac)_2]$·BNO* (Chart 1) consisting of a large magnetic anisotropic Co^{II} ion and a chiral triplet biradical ligand. This compound has one-dimensional chain structure and displays unusual magnetic behavior under the influence of a magnetic field.

Chart 1. $[Co(hfac)_2]$·BNO*

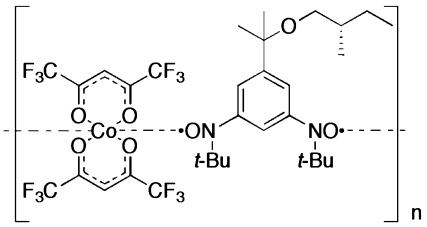

Experimental Section

General Procedures and Materials. 1−3 and **6** were synthesized under N_2 atmosphere and using freshly distilled solvents. $[Co(hfac)_2(H_2O)_2]$ was prepared according to a literature method.[14] All starting reagents are available commercially. Organic compounds were characterized by NMR measurements.

Preparation of 1,3-Dibromo-5-{(1′-hydroxy-1′-methyl)ethyl}benzene (6). To a solution of 1,3,5-tribromobenzene (2.00 g, 6.35 mmol) in 30 mL of distilled diethyl ether was slowly added a 1.46 M *tert*-butyllithium (8.86 mL, 13.02 mmol) *n*-pentane solution at −78 °C, and the mixture was warmed to −30 °C and stirred for 2 h. Distilled acetone (0.5 mL, 6.67 mmol) was added to the solution, and the new solution was stirred for 4 h. After addition of an aqueous solution of NH_4Cl and diethyl ether, the organic layer was separated, washed with water, dried over anhydrous $MgSO_4$, and concentrated under reduced pressure. The orange oil was chromatographed on silica gel and *n*-hexane as eluent at first and subsequently flashed with diethyl ether. The diethyl ether fraction was concentrated and distilled under reduced pressure (5 mmHg, 105 °C) to give 1.54 g (82.5%) of **6** as colorless crystals. ^{1}H NMR (400 MHz, $CDCl_3$): δ 7.55 (d, 2H), 7.53 (d, 1H), 1.54 (s, 6H).

Preparation of (*S*)-((2-Methylbutyl)oxyl)toluenesulfonyl (5). To a solution of *p*-toluenesulfonyl chloride (8.87 g, 46.5 mmol) in 20 mL of pyridine was added (*S*)-3-methyl-1-butanol (5.0 mL, 46.5 mmol), which was then stirred at 0 °C for 1 day. To this suspension, water and *n*-hexane were added and separated. The organic layer was neutralized with dilute hydrochloric acid and separated again. The organic layer was dried over with $MgSO_4$ and $NaHCO_3$, filtered, and concentrated under reduced pressure to give 9.50 g (84.7%) of **5** as a colorless oil. ^{1}H NMR (400 MHz, $CDCl_3$): δ 7.78 (d, 2H), 7.34 (d, 2H), 3.84 (m, 2H), 2.45 (s, 3H), 1.71 (m, 1H), 1.39 (m, 1H), 1.14 (m, 1H), 0.87 (d, 3H), 0.82 (t, 3H).

Preparation of 1,3-Dibromo-5-{1′-methyl-1′-[2″-(*S*)-methylbutoxy]ethyl}benzene (4). To a solution of **6** (1.0 g, 3.40 mmol) in 20 mL of diethylene glycol dimethyl diethyl ether (diglyme) was added ground KOH (85%) powder (422 mg, 6.80 mmol) in small fractions, and the solution was stirred for 2 h at room temperature. After the color of the solution changed to red, it was warmed to 110 °C. A solution of **5** (0.82 g, 3.40 mmol) in 20 mL of diglyme was slowly added to the mixture during 3 h, and the new solution was stirred until the color

(8) (a) Caneschi, A.; Gatteschi, D.; Sessoli, R.; Barra, A. L.; Brunel, L. C.; Guillot, M. *J. Am. Chem. Soc*. **1991**, *113*, 5873. (b) Gatteschi, D.; Sessoli, R. *Angew. Chem., Int. Ed*. **2003**, *42*, 268. (c) Gatteschi, D.; Sessoli, R.; Villain, J. *Molecular Nanomagnets*; Oxford University Press: New York, 2006.

(9) (a) Caneschi, A.; Gatteschi, D.; Lalioti, N.; Sessoli, R.; Venturi, G.; Vindigni, A.; Rettori, A.; Pini, M. G.; Novak, M. A. *Angew. Chem., Int. Ed*. **2001**, *40*, 1760. (b) Miyasaka, H.; Clérac, R. *Bull. Chem. Soc. Jpn*. **2005**, *78*, 1725. (c) Kajiwara, T.; Nakano, M.; Kaneko, Y.; Takaishi, S.; Ito, T.; Yamashita, M.; Igashira-Kamiyama, A.; Nojiri, H.; Ono, Y.; Kojima, N. *J. Am. Chem. Soc*. **2005**, *127*, 10150. (d) Ishii, N.; Ishida, T.; Nogami, T. *Inorg. Chem.* **2006**, *45*, 3837. (e) Bernot, K.; Bogani, L.; Caneschi, A.; Gatteschi, D.; Sessoli, R. *J. Am. Chem. Soc*. **2006**, *128*, 7947.

(10) (a) Coronado, E.; Galan-Mascaros, J. R.; Gomez-Garcia, C. J.; Laukhin, V. *Nature* **2000**, *408*, 447. (b) Yamaguchi, K.; Kawakami, T.; Taniguchi, T.; Nakano, S.; Kitagawa, Y.; Nagao, H.; Ohsaku, T.; Takeda, R. *Polyhedron* **2003**, *22*, 2077. (c) Akutsu, H.; Yamada, J.; Nakatsuji, S.; Turner, S. S. *Solid State Commun.* **2006**, *140*, 256.

(11) (a) Uji, S.; Shinagawa, H.; Terashima, T.; Yakabe, T.; Terai, Y.; Tokumoto, M.; Kobayashi, A.; Tanaka, H.; Kobayashi, H. *Nature* **2001**, *410*, 908. (b) Graham A. W.; Kurmoo M.; Day P. *J. Chem. Soc., Chem. Commun*. **1995**, 2061. (c) Kurmoo, M.; Graham, A. W.; Day, P.; Coles, S. J.; Hursthouse, M. B.; Caulfield, J. S.; Singleton, J.; Pratt, F. L.; Hayes, W.; Ducasse, L.; Guionneau, P. *J. Am. Chem. Soc*. **1995**, *117*, 12209. (d) Fujiwara, H.; Kobayashi, H. *Bull. Chem. Soc. Jpn*. **2005**, *78*, 1181.

(12) (a) Karasawa, S.; Kumada, H.; Koga, N.; Iwamura, H. *J. Am. Chem. Soc*. **2001**, *123*, 9685. (b) Ohkoshi, S.; Ikeda, S.; Hozumi, T.; Kashiwagi, T.; Hashimoto, K. *J. Am. Chem. Soc*. **2006**, *128*, 5320.

(13) (a) Caneschi, A.; Gatteschi, D.; Ray, P.; Sessoli R. *Inorg. Chem*. **1991**, *30*, 3936. (b) Hernáckz-Molina, M.; Lloret, F.; Ruiz-Pérez, C.; Julve, M. *Inorg. Chem*. **1998**, *37*, 4131. (c) Kumagai, H.; Inoue, K. *Angew. Chem., Int. Ed*. **1999**, *38*, 1601. (d) Inoue, K.; Kumagai, H.; Markosyan, A. S. *Synth. Met*. **2001**, *121*, 1772. (e) Inoue, K.; Imai, H.; Ghalasasi, P. S.; Kikuchi, K.; Ohba, M.; Okawa, H.; Yakhmi, J. V. *Angew. Chem., Int. Ed*. **2001**, *40*, 4242. (f) Andres, R.; Brissard, M.; Gruselle, M.; Train, C. *Inorg. Chem*. **2001**, *40*, 4633. (g) Ghalasasi, P. S.; Inoue, K.; Samant, S. D.; Yakhmi, J. V. *Polyhdron* **2001**, *20*, 1495. (h) Coronado, E.; Galan-Mascaros, J. R.; Gomez-Garcia, C. J.; Martínez-Agudo, J. M. *Inorg. Chem*. **2001**, *40*, 113. (i) Coronado, E.; Gómez-García, C. J.; Martínez-Agudo, J. M. *Inorg. Chem*. **2002**, *41*, 4615. (j) Inoue, K.; Kikuchi, K.; Ohba, M.; Okawa, H. *Angew. Chem., Int. Ed*. **2003**, *42*, 4810. (k) Coronado, E.; Giménez-Saiz, C.; Martínez-Agudo, J. M.; Neuz, A.; Romero, F. M.; Stoeckli-Evans, H. *Polyhedron* **2003**, *22*, 2435. (l) Imai, H.; Inoue, K.; Kikuchi, K.; Yoshida, Y.; Itoh, M.; Sunahara, T.; Onaka, S. *Angew. Chem., Int. Ed*. **2004**, *43*, 5618. (m) Coronado, E.; Galán-Mascarós, J. R.; Gómez-García, C. J.; Murcia-Martínez, A.; Canadell, E. *Inorg. Chem*. **2004**, *43*, 8072. (n) Inoue, K.; Imai, H.; Ohkoshi, S. A Chiral Molecule-Based Magnet. In *Magnetism: Magnetic Materials Vol. 5*; Miller, J. S., Drillon, M., Eds.; Wiley-VCH: Weinheim, Germany, 2005; p 41. (o) Cinti, F.; Affronte, M.; Lascialfari, A.; Barucci, M.; Olivieri, E.; Pasca, E.; Rettori, A.; Risegari, L.; Ventura, G.; Pini, M. G.; Cuccoli, A.; Roscilde, T.; Caneschi, A.; Gatteschi, D.; Rovai, D. *Polyhedron* **2005**, *24*, 2568. (p) Imai, H.; Inoue, K.; Kikuchi, K. *Polyhedron* **2005**, *24*, 2808. (q) Coronado, E.; Galán-Mascarós, J. R.; Gómez-García, C. J.; Murcia-Martínez, A. *Chem.*—Eur. J. **2006**, *12*, 3484. (r) Clemente-León, M.; Coronado, E.; Gómez-García, C. J.; Soriano-Portillo, A. *Inorg. Chem*. **2006**, *45*, 5653. (s) Coronado, E.; Gómez-García, C. J.; Nuez, A.; Romer, F. M.; Waerenborgh, J. C. *Chem. Mater*. **2006**, *18*, 2670.

(14) (a) Petrukhina, M. A.; Henck, C.; Li, B.; Block, E.; Jin, J.; Zhang, S.; Clerac, R. *Inorg. Chem*. **2005**, *44*, 77. (b) Pecsok, R. I.; Reynolds, W. D.; Fackler, J. P., Jr.; Lin, I.; Pradilla-Sorzano, J. *Inorg. Synth.* **1974**, *15*, 96.

changed to creamy yellow. To the mixture, 10 mL of water was added and separated, dried over with anhydrous $MgSO_4$, filtered, and concentrated under reduced pressure to give 773 mg (62.4%) of **4** as a colorless oil. ^{1}H NMR (400 MHz, $CDCl_3$): δ 7.53 (d, 1H), 7.47 (d, 2H), 2.95 (m, 2H), 1.59 (m, 2H), 1.47 (m, 6H), 1.12 (m, 1H), 0.88 (q, 6H).

Preparation of 1,3-Bis[*N*-*tert*-butyl-*N*-(hydroxyamino)]-5-{1′-methyl-1′-[2″-(*S*)-methylbutoxy]ethyl}benzene (3). A solution of **4** (1.0 g, 2.75 mmol) in 20 mL of diethyl ether was cooled to −78 °C, and a 1.46 M *tert*-butyllithium (7.6 mL, 11.14 mmol) *n*-pentane solution was slowly added to the solution. The mixture was warmed gradually to −30 °C and stirred for 2 h. A solution of 2-methyl-2-nitrosopropane dimer (0.49 g, 5.64 mmol) in 10 mL of diethyl ether was added in small fractions to the solution, and the new solution was stirred for 3 h at −30 °C. After addition of an aqueous solution of NH_4Cl and diethyl ether, the organic layer was separated, washed with water and dried over anhydrous $MgSO_4$, filtered, and concentrated under reduced pressure. To the mixture, a small amount of *n*-hexane was added and cooled for 1 day at −20 °C, to give 567 mg (54.2%) of a white powder of **3**. ^{1}H NMR (400 MHz, $CDCl_3$): δ 7.05 (s, 1H), 6.89 (s, 2H), 2.91 (m, 2H), 1.58 (m, 4H), 1.37 (m, 6H), 1.15 (m, 18H), 1.04 (q, 1H), 0.84 (m, 6H).

Preparation of 1,3-Bis[*N*-*tert*-butyl-*N*-(oxylamino)]-5-{1′-methyl-1′-[2″-(*S*)-methylbutoxy]ethyl}benzene (2). A solution of **3** (100 mg, 0.26 mmol) in 15 mL of dichloromethane was cooled in an ice bath to 0 °C, and to this solution was added Ag_2O (500 mg, 2.16 mmol), which was then stirred for 2 h. The mixture was purified by silica gel column chromatography with dichloromethane as eluent to give 98 mg (98%) of **2** as an orange colored oil. It was subsequently used for the next step.

Preparation of [Co(hfac)$_2$]·BNO* (1). [Co(hfac)$_2$(H$_2$O)$_2$] (132 mg, 0.26 mmol) was refluxed in *n*-hexane to remove water of hydration by azeotropic distillation. To this solution, a solution of BNO* (98 mg, 0.26mmol) in dichloromethane was added and stirred for 30 min at 80 °C. The mixture was cooled at −20 °C for 1 week to give 106 mg (47.8%) of the dark red crystals of **1**. These crystals were suitable for X-ray structure determination. Anal. Calcd for $C_{32}H_{40}CoF_{12}N_2O_7$ (**1**): C, 45.13; H, 4.73; N, 3.29. Found: C, 45.75; H, 4.05; N, 3.29. IR (KBr): ν = 1644, 1554, 1504, 1257, 1196, 1150, 795, 669, 587 cm^{-1}.

Physical Measurements. Dc and ac magnetic susceptibilities were measured by use of a Quantum Design MPMS-XL SQUID magnetometer. The magnetic susceptibilities were corrected for diamagnetism using Pascal's constants. The IR spectrum was measured on KBr disk with a Jasco FT/IR-660 plus spectrometer. The X-band ESR spectra of polycrystalline samples were measured by a Bruker ESR 500 equipped Oxford ESR 900 cryostat for the measurements at 300−15 K and ESR 910 cryostat at 15−2 K, respectively.

Crystallography. A selected single crystal of size 0.50 × 0.25 × 0.18 mm^3 was mounted on a glass fiber. The X-ray data were collected at 100 K using a Bruker SMART-APEX diffractmeter, equipped with a CCD area detector and graphite-monochromated Mo Kα radiation, λ = 0.710 73 Å, employing a ω-scan mode (0.3° step) and semiempirical absorption correction on Laue equivalents. The structure was solved by direct methods and refined by full-matrix least squares against F^2 of all data, using SIR-97 and SHELXTL softwares.[15,16] All non-hydrogen atoms were refined anisotropically. All hydrogen atoms were placed in calculated positions and not refined. The refinement converges with R1 = 7.14% for 7856 data ($I > 4\sigma(I)$), wR2 = 19.60% for 9717 unique data ($1.18 \leq \theta \leq 28.39$), Flack parameter = −0.03(2), and maximim/minimum residual electron density 1.34/−1.03 e Å^{-3}.

(15) Altamore, A.; Burla, M. C.; Camalli, M.; Gascarano, G. L.; Giacovazzo, C.; Guaglirdi, A.; Molitemi, G. G.; Polidori, G.; Spagna, R. SIR-97. *J. Appl. Crystallogr.* **1999**, *32*, 115.
(16) Sheldrick, G. M. *SHEXL-97*; University of Göttingen: Göttingen, Germany, 1997.

Table 1. Crystallographic Data for **1**

formula	$C_{32}H_{40}CoF_{12}N_2O_7$
mol wt	851.59
cryst system	triclinic
space group	$P\bar{1}$ (No. 1)
a, Å	10.704(4)
b, Å	11.573(5)
c, Å	17.429(7)
α, deg	81.647(7)
β, deg	84.643(7)
γ, deg	63.195(6)
V, Å^3	1905.6(14)
Z	2
no. of unique reflcns	9717
no. of reflcns used	7856
GOF	1.000
R1 (wR2)	0.0714 (0.1960)
Flack factor	−0.03(2)

Results and Discussion

Crystal Structure. X-ray structural analysis of **1** revealed the absence of all symmetry, and thus, the triclinic *P*1 (No. 1) space group was chosen. Details of crystallographic data are presented in Table 1. In the unit cell, there are two crystallographically independent units of [Co(hfac)$_2$]·BNO*. [Co(hfac)$_2$] and the BNO* radical form a uniform one-dimensional *R*-type helical chain structure along the crystallographic *c*-axis. Figure 1 presents a view of the 1-D chain structure. In the unit cell, there is only one helical chain consisting of the two different building blocks of [Co(hfac)$_2$]·BNO*. The aminoxyl groups of BNO* are rotated out of the phenylene ring plane. The chiral substitute of all BNO* molecules have the *S*-configuration. These alkyl groups are situated between the 1-D chains; therefore, the chains are well isolated from each other (Figures 2 and 1S). All cobalt ions exhibit octahedral coordination with the four oxygen atoms of two hfac ligands in the equatorial plane and the two oxygen atoms of the aminoxyl groups of two different BNO* molecules in trans- configurations. The Co−O$_{hfac}$ bond lengths range from 2.037(5) to 2.056(6) Å, and Co−O$_{rad}$ ranges from 2.075(6) to 2.096(6) Å. The bond angles made

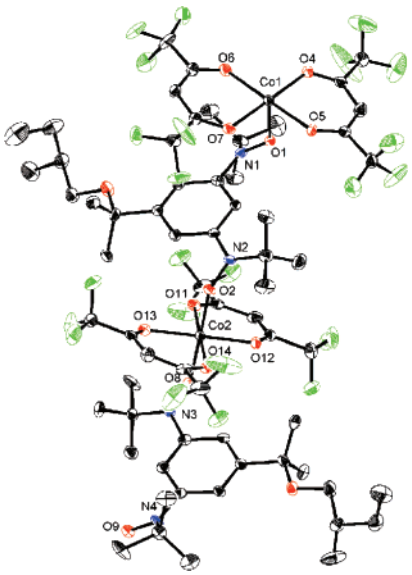

Figure 1. ORTEP drawing of the crystallographically independent unit of **1**. Thermal ellipsoids are at the 40% level. H atoms are omitted for clarity. Two Co and some selected atoms are labeled. Key: black, carbon; red, oxygen; blue, nitrogen; green, fluorine.

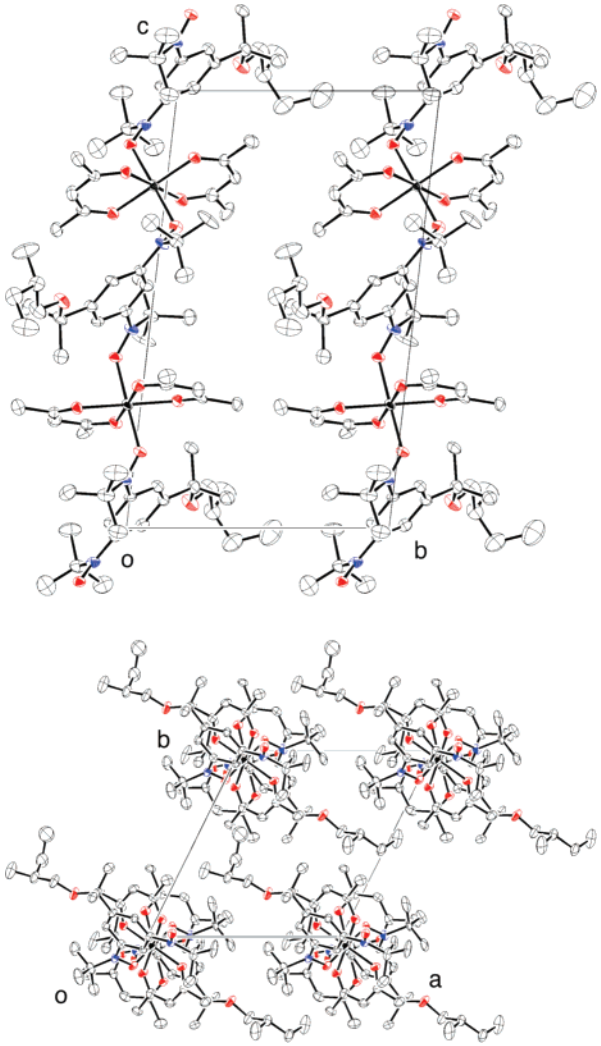

Figure 2. Projection of crystal structure of **1** along the *a*-axis (top) and *c*-axis (bottom). H and F atoms are omitted for clarity. Key: red, oxygen; blue, nitrogen.

by two oxygen atoms located at the diagonal corners of the coordination octahedra and central Co ion are almost 180°. (The angles lie in the range 178.4(3)−179.5(3)°.) The intrachain Co−Co distances of Co(1)−Co(2) and Co(2)−Co(1′) are 8.722 and 8.696 Å, respectively; additionally, the shortest interchain Co−Co distance is 10.697 Å. Other selected Co−Co distances are given in the Supporting Information (Figure 2S). Selected bond lengths, bond angles, torsion angles, and intrachain Co−Co distances are given in Tables 2 and 1S.

Magnetic Properties. The *m*-phenylenebis(nitroxide) radical has previously been shown to have the triplet ground state where its intramolecular ferromagnetic interaction, J_1/k_B, is large (430 K) for the nonchiral BNO^H (BNO^H = 1,3-bis(*N*-*tert*-butyl-*N*-(oxylamino))benzene).[17] The magnetic interaction between nitroxide radical and Co^{II} ion (J_2) appears to be antiferromagnetic owing to the overlapping of magnetic orbitals of the nitroxide radical and Co^{II}. This value is not available in the literature, and the observed susceptibility suggests $J_2 \ll 0$.[18]

All magnetic measurements were performed for the polycrystalline samples. The $\chi_m T$ vs T and $1/\chi_m$ vs T plots are presented in Figure 3. The temperature dependence of $\chi_m T$ has a minimum at 220 K, which suggests ferrimagnetic behavior due the antiparallel alignment of the noncompensated moments within each chain in **1**. Weiss temperature, Θ, which was estimated to be −89.9 K from the $1/\chi_m$ vs T plot in the temperature range 220−300 K, indicates $J_2 \ll 0$. The peak temperature in the $M-T$ curve is around 20 K and shifts to lower temperatures by increasing the dc field (Figure 3S).

The magnetic susceptibilities for the zero-field-cooled (χ_{ZFC}) sample and field-cooled sample (χ_{FC}) were measured in applied fields of 500 and 5000 Oe (Figure 4). In 500 Oe, χ_{ZFC} and χ_{FC} exhibit similar values in the temperature region 4−100 K. At temperatures $4 < T < 16$ K, a shoulder is evident for both χ_{ZFC} and χ_{FC} curves. At 4 K, the χ_{ZFC} value increases abruptly; subsequently, it saturates and decreases gradually with further increasing temperature. Below 4 K, $\chi_{ZFC}(T)$ and $\chi_{FC}(T)$ are split and demonstrate constant values below 3.2 K. In 5000 Oe, the χ_{ZFC} value is also a constant in the temperature range 2−3.2 K, but the peak at 20 K is not present, suggesting reversal of all moments in this high field. The sharp drop in the susceptibility in 500 Oe suggests long-range magnetic ordering of the resultant moments within each chain. However, as the Co^{II} ion becomes more anisotropic as the temperature is lowered due to the depopulation of the upper Kramers doublets, a small canting is generated resulting in the weak ferromagnetism below 4 K with consequent magnetic hardness.

The different kinds of hysteresis loops were observed from 1.8 to 30 K. In the temperature interval 4−18 K, the isothermal magnetization, $M(H)$ dependence (shown in Figure 5a) seem to be typical for antiferromagnets revealing a metamagnetic transition under application of an external field. This field-induced phase transition occurs when an applied field reaches a critical value of the order of the AF interchain exchange. The saturated magnetization value (M_S) of **1** is approximately 1.16 μ_B/formula unit. This value is higher than that expected (1 μ_B if the average g-value of Co is 2 and $S = 3/2$ or 0.15 μ_B if the average g-value of Co is 4.3 and $S = 1/2$) for a simple ferrimagnetic model consists of the unit of Co^{II} and BNO* ($S = 1$) which are coupled antiferromagnetically. As shown in Figure 5a, the phase transition from the AF state to the forced ferrimagnetic (FoFi) state around 850 Oe is accompanied by hysteresis. However, the width of the hysteresis, ΔH_c, does not exceed the critical field and the remnant magnetization remains zero above 4 K; that is, the magnet remains soft. However, when the temperature is set below 4 K, the width of the hysteresis loop increases abruptly leading to the constricted shape of the loop at temperatures $3.6 \text{ K} < T < 4$ K (see Figure 5b) and to the "magnet-type" hysteresis loop with further lowering of temperature (shown in Figure 5c). The coercive field reaches a value of 25 kOe below 2.6 K. This behavior has some characteristics as those observed for $Co_2(OH)_2$(terephthalate) and Co_2(pyromellitate).[19c]

Additionally, the hysteresis loops measured in the ranges 1.8−2.8, 2−3.8, and 4−22 K are shown in Figure 5S. It is considered that the change of the shape and large increase of the width of the hysteresis loops with decreasing temperature below 4 K

(17) (a) Calder, A.; Forrester, Alexander, R.; James, P. G.; Luckhurst, G. R. *J. Am. Chem. Soc.* **1969**, *91*, 3724. (b) Hosokoshi, Y.; Katoh, K.; Nakazawa, Y.; Nakano, H.; Inoue, K. *J. Am. Chem. Soc.* **2001**, *123*, 7921.
(18) Field, L. M.; Morón, M. C.; Lahti, P. M.; Palacio, F.; Paduan-Filho, A.; Oliveira, N. F. *Inorg. Chem.* **2006**, *45*, 2562.

Table 2. Selected Bond Lengths (Å), Bond Angles (deg), and Intrachain Co−Co Distances (Å) of **1**

Co1				Co2			
Co1−O1	2.075(6)	N1−O1	1.303(9)	Co2−O2	2.093(5)	N3−O8	1.283(9)
Co1−O9	2.081(5)	N2−O2	1.296(9)	Co2−O8	2.096(6)	N4−O9	1.286(9)
Co1−O4	2.054(6)	Co1−Co2	8.722	Co2−O11	2.037(5)	Co2−Co1	8.696
Co1−O5	2.048(5)			Co2−O12	2.046(5)		
Co1−O6	2.056(6)			Co2−O13	2.040(6)		
Co1−O7	2.049(6)			Co2−O14	2.056(6)		
O1−Co1−O9	179.1(3)	O4−Co1−O6	91.0(2)	O11−Co2−O14	179.0(3)	O8−Co2−O12	86.5(2)
O4−Co1−O7	179.5(3)	O4−Co1−O9	93.7(2)	O12−Co2−O13	178.4(3)	O8−Co2−O13	94.0(2)
O5−Co1−O6	179.3(3)	O5−Co1−O7	92.2(2)	O2−Co1−O8	179.3(3)	O8−Co2−O14	95.1(2)
O1−Co1−O4	86.1(2)	O5−Co1−O9	93.4(2)	O2−Co2−O11	95.9(2)	O11−Co2−O12	88.5(2)
O1−Co1−O5	85.7(2)	O6−Co1−O7	88.5(2)	O2−Co2−O12	94.4(2)	O11−Co2−O13	93.1(2)
O1−Co1−O6	94.6(2)	O6−Co1−O9	86.3(2)	O2−Co2−O13	85.2(2)	O12−Co2−O14	90.7(2)
O1−Co1−O7	93.8(2)	O7−Co1−O9	86.4(2)	O2−Co2−O14	84.8(2)	O13−Co2−O14	87.7(2)
O4−Co1−O5	88.3(2)			O8−Co2−O11	84.2(2)		

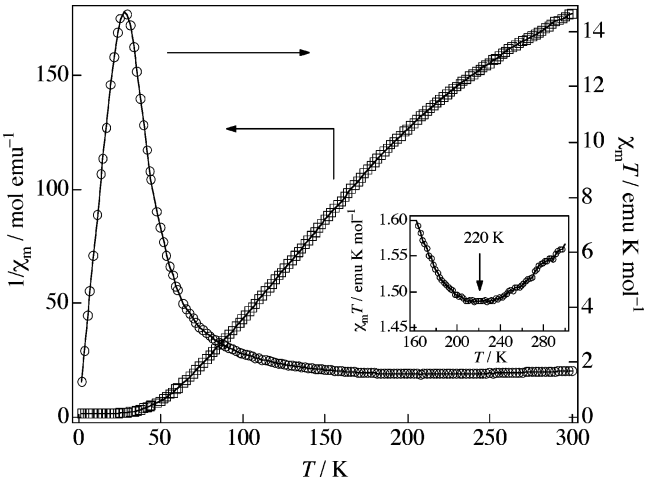

Figure 3. Temperature dependence plots of $1/\chi_m$ (crosses) and $\chi_m T$ (open circles) for **1**. Inset: Expanded $\chi_m T$ curve around the minimum point.

originates from freezing of domain wall displacement due to the crossover from a Heisenberg-type antiferromagnet to an Ising-type antiferromagnet.[19,20] Figure 8S shows ESR spectra measured at selected temperatures and the plot of the positions of *g*-values of the half-width of left end peaks. At 300 K, it shows only one signal at $g = 2.00$. Upon lowering of the temperature, the peaks were split and the *g*-value increased. In Figure 8Sc, the *g*-value shifts following a decrease temperature show a two times increase at around 70 and 7 K. It is considered that they are originated from the magnetic interactions and single ion anisotropy of Co(II).

In the temperature dependence of the ac magnetic susceptibility measurements in zero magnetic field, the χ_{ac}' values show a frequency dependence in the temperature range 4−8 K. These data support our suggestion about the crossover from Heisenberg-type to Ising-type regime occurred in this temperature

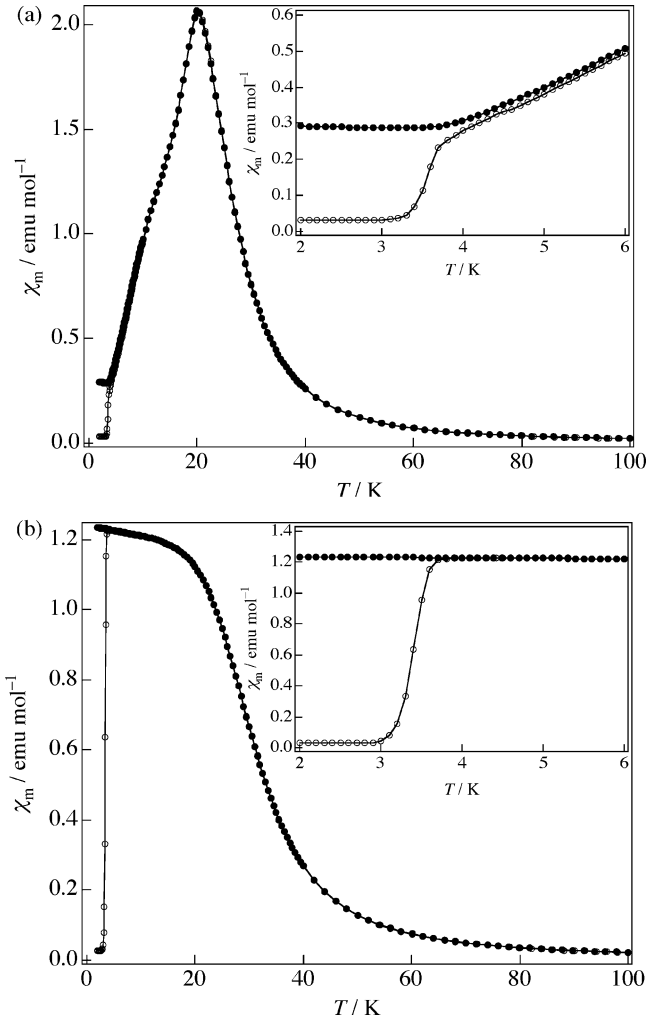

Figure 4. Temperature dependence of molar magnetic susceptibility measured at 500 Oe (a) and 5000 Oe (b) employing the ZFC (open circles) and FC (closed circles) mode. The inset shows a magnified view at the temperature region 2−6 K.

range.[19,20] The position of the χ_{ac}' peak at around 20 K is observed to be frequency independent (Figure 6S). The $\chi_{ac}''(T)$ values dependence shows an additional peak which is frequency dependent (1−1500 Hz) (Figure 6S). In a bias magnetic field of 500 Oe which is lower than the metamagnetic critical field, χ_{ac}' and χ_{ac}'' show behavior similar to that in 0 Oe (Figure 6S). The frequency-dependent region of χ_{ac}' broadens with increasing

(19) (a) Kurmoo, M.; Kumagai, H.; Green, M. A.; Lovett, B. W.; Blundell, S. J.; Ardavan, A.; Singleton, J. *J. Solid State Chem.* **2001**, *159*, 343. (b) Lovett, B. W.; Blundell, S. J.; Kumagai, H.; Kurmoo, M. *Synth. Met.* **2001**, *121*, 1814. (c) Kumagai, H.; Kepert, C. J.; Kurmoo, M. *Inorg. Chem.* **2002**, *41*, 3410. (d) Kurmoo, M.; Kumagai, H.; Hughes, S. M.; Kepert, C. J. *Inorg. Chem.* **2003**, *42*, 6709.

(20) (a) Miller, J. S.; Calabrese, J.; McLean, R. S.; Epstein, A. J. *Adv. Mater.* **1992**, *4*, 498. (b) Miller, J. S.; Vazquez, C.; Jones, N. L.; McLean, R. S.; Epstein, A. J. *J. Mater Chem.* **1995**, *5*, 707. (c) Wynn, C. M.; Gîrţu, M. A.; Sugiura, K.; Brandon, E. J.; Manson, J. L.; Miller, J. S. Epstein A. J. *Synth. Met.* **1997**, *85*, 1695. (d) Wynn, C. M.; Gîrţu, M. A.; Miller, J. S.; Epstein, A. J. *Phys. Rev. B* **1997**, *56*, 14050. (e) Dawe, L. N.; Miglioi, J.; Turnbow, L.; Taliafferro, M. L.; Shum, W. W.; Bagnato, J. D.; Zakharov, L. N.; Rheingold, A. L.; Arif, A. M.; Fourmigué, M.; Miller, J. S. *Inorg. Chem.* **2005**, *44*, 7530.

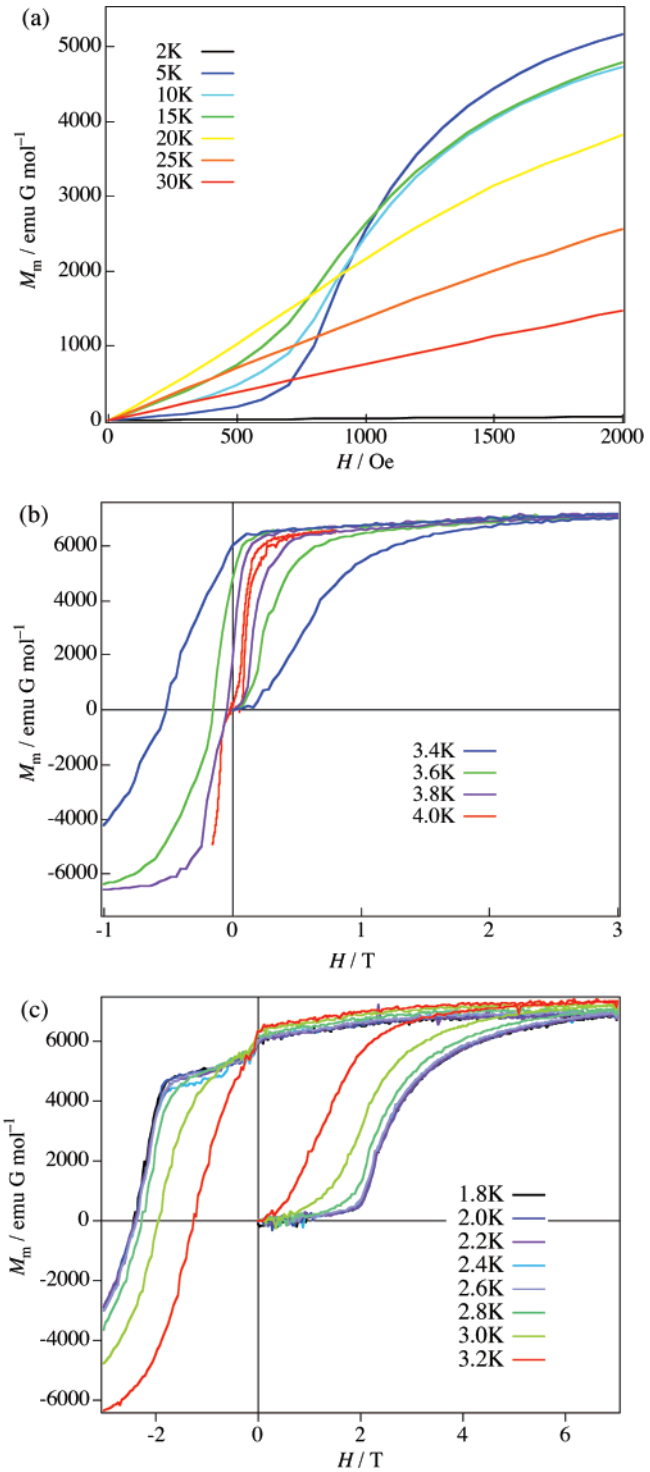

Figure 5. Temperature dependence of hysteresis loops measured at selected temperatures: (a) 2−30 K; (b) 3.4−4.0 K; (c) 1.8−3.2 K.

strength of dc magnetic field above 500 Oe. The χ_{ac}'' peak in the vicinity of 4−6 K corresponds to the phase transition from AF to field-induced ferrimagnetic (FiFi) phase (vide infra). The behaviors of χ_{ac}' and χ_{ac}'' are completely different in the dc field of 5000 Oe, i.e., in a field well over the metamagnetic critical field. The χ_{ac}' values show a sharp rise at around 5 K and a frequency-independent peak at around 30 K (Figure 6S). The peaks at 30 K correspond to the phase transition from paramagnetic state to forced ferrimagnetic state.

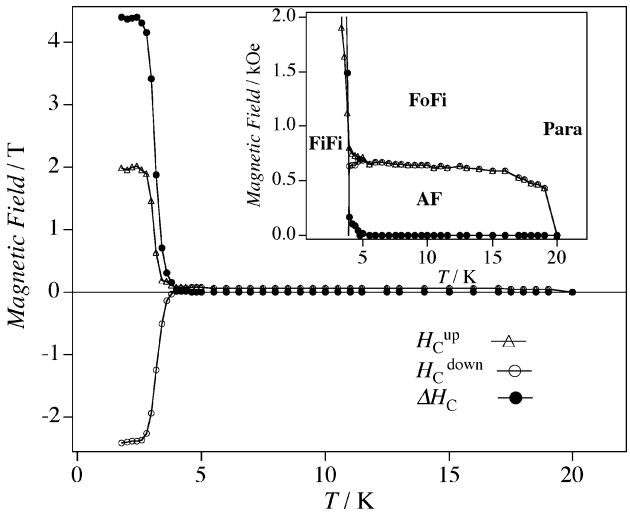

Figure 6. Magnetic phase diagram of **1**. Inset: Diagram magnified from 0 to 2000 Oe.

The change of the magnetization with magnetic field reveals a different dynamics below and above this crossover temperature. It is clearly seen from dc field dependence of the ac susceptibility presented in Figure 6Sa,b at selected temperatures. At $T \geq 20$ K, the behavior of the ac susceptibility is quite typical for paramagnets (Figure 7Sg). There is no frequency dependence of the χ_{ac}' and χ_{ac}'' curves within the frequency range used (1−1000 Hz). The imaginary part of the ac susceptibility is zero, since the relaxation time of magnetic moments above the ordering temperature is significantly smaller than the period of ac magnetic field. Below the ordering temperature, the imaginary part of the ac susceptibility reflects mainly the energy losses, which occur during the magnetization rotation within the domain and domain wall movement. At 7.5 K, i.e., above the crossover temperature, the $\chi_{ac}'(H_{dc})$ dependence shows frequency-dependent peaks at around 850 Oe and χ_{ac}'' curves also show field-dependent peak (Figure 7Sd). This peak indicates the spin-flip transition, which is associated with the nucleation of the FoFi phase within AF phase and displacement of the domain walls separating AF and FoFi phases. The frequency dependence of both χ_{ac}' and χ_{ac}'' in the vicinity of the critical field becomes more pronounced with decreasing temperature especially in the low-frequency range. This means that the rate of the magnetization change decreases with lowering temperature. Finally, below 4 K, we could not observe any peak of the χ_{ac}' and χ_{ac}'' in the vicinity of the field-induced AF−FiFi transition in $M-H$ measurements below 4 K (Figure 7Sa,b). These data are indicative of the domain wall freezing below the crossover temperature. $\chi_{ac}-H$ plots at 12, 10, and 5 K are presented in Figure 7Sf,e,c. To understand its magnetic properties more clearly, the magnetic phase diagram was constructed.

Magnetic Phase Diagram. The magnetic phase diagram in the low-temperature region is displayed in Figure 6. Three lines in the phase diagram, H_C^{up} (critical field of the initial magnetization process), H_C^{down} (critical field of the demagnetization process), and ΔH_C (difference between H_C^{up} and H_C^{down}) represent the boundary of the FiFi phase,[20,21] the FoFi phase, and AF phase, respectively. The H_C^{up} curve corresponds to the

(21) (a) Baranov, N. V.; Pirogov, A. N.; Teplykh, A. E. *J. Alloys Compd.* **1995**, *226*, 70. (b) Baranov, N. V.; Mushnikov, N. V.; Goto, T.; Hosokoshi, Y.; Inoue, K. *J. Phys.: Condens. Matter* **2003**, *15*, 8881.

spin-flip field. This diagram exhibits four magnetic ground states. The paramagnetic state exists above 20 K. In the temperature region 4−20 K, this molecule behaves as a usual metamagnet. The value of the critical field of the AF−FoFi transition corresponds to the interchain exchange interaction. An upturn of ΔH_C with decreasing temperature below 4 K is associated with freezing of the domain wall motion in the Ising-type magnetic structure. Below 3.2 K, the compound displays a large coercive field (ca. 25 kOe at 2 K) and hysteresis loop that seem to be typical for hard magnetic materials. After application of a strong magnetic field in this temperature range, further variation of an external field does not lead to the regime of the initial AF state in the compound. Thus, this FiFi state is a metastable state. The width of the hysteresis loops in the Ising state is controlled by the exchange interaction within chains and thermal activation of the domain wall displacement. However, the increase of the width of the hysteresis loops with decreasing temperature is stopped below ∼2.8 K, which can be ascribed to the change in the mechanism of the domain wall displacement from the thermal activation to macroscopic quantum tunneling.

To get an insight into the plausible orientation of the moments in the different ground state, we looked for different models to account for the observed magnetization values. Above 20 K, the compound is in the paramagnetic state with strong intramolecular ferromagnetically coupled $S = 1/2$ radicals and less strong antiferromagnetically coupling between the cobalt moment and the radicals. At 20 K, long-range magnetic ordering is observed with a residual moment of 0.03 μ_B. This value is obtained from the χ_m values of below 3 K (Figure 4). This value is much smaller than the 0.3 μ_B expected for a ferrimagnetic state, that is, all the cobalt moments being antiparallel to those of the radicals assuming the moment of cobalt to be 2.3 μ_B ($S = 1/2$, $g > 4$) and that of the radical is 2.0 μ_B ($S = 1$, $g = 2.0$). The presence of small residual moment may result from several origins: (i) the lack of the compensation of magnetic moments at the ends of magnetically broken chains due the presence of nonmagnetic impurities and lattice defects;[22] (ii) the pinning of domain walls separating AF and F phases on nonmagnetic impurities and lattice defects after zeroing the field; (iii) the presence of canted antiferromagnetic structure with a weak ferromagnetic component. If one bears in mind the high anisotropy of Co, the presence of a small canting of the moment between two sublattices, where one sublattice comprises one Co atom and a pair of radicals, seems to be reasonable. The estimated canting is 5.7° from the easy axis, if we assume that both the cobalt and the radical moments are canted by the same angle. The double of this angle can be a measure of the angle between the directions of the moments of the two crystallographic independent cobalt atoms. The observed angle between O−Co−O (where the oxygen atoms are those of the radicals) is 11.7°. This agreement, though coincidental, may suggest that the moments of the cobalt atoms is quite likely perpendicular to the $Co(hfac)_2$ plane. The second magnetization value of 1.16 μ_B is that observed upon application of field larger than the critical metamagnetic field. This is larger than that of the ferrimagnetic state (0.3 μ_B) but smaller than that of a ferromagnetic state (4.3 μ_B) with parallel alignment of magnetic moments of Co ions and radicals. For the polycrystalline sample we have to obtain at least half (2.15 μ_B) of the saturation value in the case of uniaxial magnetocrystalline anisotropy. Therefore, one can suggest that in our case all the moments are tilted. Assuming same tilt angle for both Co and radicals, as we did above, the estimated tilt angle is 74° from the hard axis. This may be the reason for the very square shape hysteresis loop with a low saturation value. The tilt may be regarded as a fan, which may well be chiral. Neutron diffraction, if ever a fully deuterated sample becomes available, may resolve the problem.

Conclusion

We successfully synthesized a novel organic−inorganic hybrid type chiral structural antiferromagnet, which is comprised of $[Co(hfac)_2]$ and a chiral triplet bis(nitroxide) radical. This magnet possesses 1-D helical chain structure; additionally, the structure is characterized by *R*-type helicity. Initially, in the high-temperature region above 20 K, this molecule displays behavior as a paramagnetic state. Below 20 K, antiferromagnetic interaction dominates among 1-D ferrimagnetic chains, and the ground state of this compound is 3-D antiferromagnetic. In the temperature range 3.2−20 K, this compound behaves as a metamagnet and its M_S is ∼1.16 μ_B. However, below ∼4 K, the thermal activated motion of the domain wall between the AF and FoFi phases is frozen owing to the high single ion anisotropy. It is considered that this behavior is caused by crossover from a Heisenberg-type to an Ising-type antiferromagnet with decreasing temperature. The ESR spectra show *g*-value shifts, and the plot of the position of half-width of the left end peak shows a two time increase at around 70 and 7 K. It is expected that they originated from magnetic interactions and the change of single ion anisotropy of Co(II) from Heisenberg-type to Ising-type AF state. As a result, a sample undergoing magnetization by application of a high magnetic field remains in the field-induced ferrimagnetic FiFi state after removing the field. Moreover, further variation of the field does not return the sample to the initial AF state.[19−21] The initial AF alignment of the magnetic moments of the chains may be reinstated upon heating the sample above 5 K, followed by cooling in zero field. In the FiFi phase, the sample demonstrates hard magnetic properties characterized by coercive field of 25 kOe below 3 K and with $M_S \sim 1.16$ μ_B. With decreasing temperature below ∼2.5 K, the width of the hysteresis loop becomes temperature independent (Figure 4S). Above 2.5 K, the widths of the hysteresis loops show remarkable temperature dependence. These results are indicative of crossover of the thermal activated domain wall motion with quantum tunneling behavior in Ising-type magnets.[9,23] Currently, the magnetic properties of this molecule are under investigation and its magnetic phase transitions are being identified systematically. Subsequently, the magnetic properties of single crystals must be examined. Furthermore, neutron diffraction measurements are necessary to establish the relationship between magnetic properties and chirality.

Acknowledgment. We thank Dr. J. Nishijyo, Institute for the Molecular Science, for his great help with the SQUID measurements and Mr. M. Fujiwara, Institute for the Molecular Science, for his great help with ESR measurements. In crystal structural

(22) Bacerra, C. C.; Paduan-Filho, A.; Palacio, F. *J. Phys.: Condens. Matter* **2000**, *12*, 6207.
(23) (a) Lhotel, E.; Khatsko, E. N.; Paulsen, C. *Phys. Rev. B.* **2006**, *74*, 020402. (b) Yuan, S.; Raedt, H. D.; Miyashita, S. *J. Phys. Soc. Jpn.* **2006**, *75*, 084073.

analysis, we were indebted to Yadokari-XG software. This work is supported by a Grant-in-Aid for Science Research (A) (No. 18205023) from the Ministry of Education, Science, Sports, and Culture. A part of this work was supported by a "Nanotechnology Support Project" of the Ministry of Education, Culture, Sports, Science, and Technology (MEXT) of Japan.

Supporting Information Available: X-ray crystallographic information files (CIF) for **1**, magnetic properties, and crystal structures. This material is available free of charge via Internet at http://pubs.acs.org. Crystallographic data for **1** (CCDC-603148) can be also be found free of charge via www.ccdc.cam.ac.uk/conts/retrieving.html (or from Cambridge Crystallographic Centre, 12 Union road, Cambridge CB2 1EZ, U.K.; fax (+44) 1223-336-033).

JA064828I